RSC Applied Interfaces

ROYAL SOCIETY OF CHEMISTRY

PAPER

View Article Online
View Journal | View Issue

Cite this: *RSC Appl. Interfaces*, 2025, **2**, 550

Particle arrangement control and mechanical robustness enhancement of structurally coloured photonic balls composed of SiO_2 particles for environmentally benign inorganic colourants†

Takahiro Yamanaka, [a] Yuta Nakatani,[a] Kaho Itoh,[a] Naoki Tarutani, [a] Kiyofumi Katagiri, *[a] Kei Inumaru [a] and Yukikazu Takeoka [b]

Structurally coloured materials composed of monodisperse particles have attracted considerable attention as environmentally benign colourants. However, these materials exhibit poor mechanical robustness and colour degradation. Although efforts have been made to enhance the mechanical properties of structurally coloured materials, research specifically focusing on their mechanical robustness remains limited. This study investigates the preparation and mechanical robustness of structurally coloured photonic balls (PBs) composed of SiO_2 particles, emphasising the effects of preparation parameters on the particle arrangement and structural colour. We systematically varied the pH and ionic strength of SiO_2 dispersions, alongside the preparation temperatures, to examine their effects on the particle arrangement within PBs. The results indicated that at pH values near the isoelectric point, PBs adopted a colloidal amorphous-type structure, whereas higher pH levels led to colloidal crystalline-type arrangements characterised by vivid structural colours. Notably, increasing the ionic strength transitioned the particle arrangement towards a more disordered state, further emphasising the critical role of surface charge dynamics. In terms of mechanical robustness, the colloidal crystalline-type structures were stronger than their colloidal amorphous-type counterparts. The incorporation of a water-soluble silane compound as a binder in PBs significantly enhanced the interparticle necking formation during heat treatment, thereby improving the mechanical robustness. This study highlights the potential of optimising the preparation conditions for structurally coloured PBs with enhanced mechanical properties, offering a promising alternative to traditional inorganic pigments.

Received 26th October 2024,
Accepted 17th January 2025

DOI: 10.1039/d4lf00366g

rsc.li/RSCApplInter

Introduction

Colours that permeate our surroundings profoundly influence various aspects of our daily lives, including art and design, nature, and consumer products.[1,2] Most industrially produced colourants are derived from organic and inorganic compounds, predominantly pigments and dyes. Organic dyes and pigments, while often vibrant, are susceptible to fading owing to environmental factors such as light irradiation and thermal exposure. In comparison, inorganic compounds generally exhibit superior weatherability and stability. However, a significant drawback of inorganic pigments is the incorporation of heavy metals such as Pb, Cd, and Cr, which are toxic to human health and pose a considerable environmental burden. Consequently, their use is strictly regulated by Pollutant Release and Transfer Register (PRTR) laws and other international regulations.[3–5]

In the natural world, certain organisms and objects, such as Morpho butterflies and opals,[6,7] exhibit colours derived from mechanisms distinct from those of conventional pigments and dyes.[8,9] This phenomenon, referred to as structural colour, arises from the intricate physical interactions of light with submicroscale structures.[8] The diversity of materials that can generate structural colours is vast, indicating potential for replacing traditional pigments with environmentally benign alternatives. Structurally coloured materials can be categorised into several types, including multilayered structures, particle arrays, and circular polarisations. Among these, arrays of uniformly sized spherical particles are particularly noteworthy because they can effectively exhibit structural colours.[10,11]

[a] *Graduate School of Advanced Science and Engineering, Hiroshima University, 1-4-1 Kagamiyama, Higashi-Hiroshima 739-8527, Japan.*
E-mail: kktgr@hiroshima-u.ac.jp
[b] *Graduate School of Engineering, Nagoya University, Furo-cho, Chikusa-ku, Nagoya 464-8603, Japan*

† Electronic supplementary information (ESI) available. See DOI: **https://doi.org/10.1039/d4lf00366g**

In the context of colloidal particle array-type structurally coloured materials, the arrangement of particles plays a pivotal role in determining the observed visual colour.[12–16] Particle arrangements can be classified into two primary types: colloidal crystalline structures, which possess long-range order, and colloidal amorphous structures, which possess only short-range order. On flat plates, colloidal crystalline arrangements generate a vivid structural colour characterised by iridescence, meaning their appearance changes with the viewing angle, whereas colloidal amorphous structures yield matte and noniridescent colours that remain consistent regardless of the viewing angle.

Spherical colloidal clusters, which are commonly referred to as photonic balls (PBs; Fig. 1), consist of spherical colloidal particles with submicrometre sizes that assemble in a spherically symmetric manner.[11,17–26] PBs can exhibit a noniridescent structural colour that remains consistent regardless of the particle arrangement when viewed directly by the human eye; moreover, they can be handled as powders, similar to conventional inorganic pigments.[19,21,22,27] For example, it has been demonstrated that by preparing PBs with monodispersed SiO_2 particles of various diameters, structural colours of all hues can be obtained, which can be used to create colourful illustrations of weevils.[11] Additionally, it has also been reported that by combining PBs with a photochromic dye, diarylethene, which undergoes reversible isomerization upon light irradiation, the vividness of the structural colour characteristics of the PBs can be altered by light exposure.[11] Therefore, PBs have the potential to serve as practical novel colorants, replacing traditional inorganic pigments based on metal oxides. Within PBs, the arrangement of particles is as critical as the structurally coloured coatings formed on flat surfaces. PBs can be further divided into several categories according to the arrangement of their primary particles, including single face-centred cubic (FCC) crystals, layered FCC structures (often described as onion-like structures), and icosahedral, decahedral, and colloidal amorphous structures.[22,27,28] Recently, Ohnuki *et al.* reported detailed analyses of the optical properties of various types of PBs, revealing the relationship between SiO_2 particle size and optical properties, the differences in the appearance of structural colours in each category, as well as the reasons why iridescence observed in planar colloidal crystals is suppressed in PBs.[18,22]

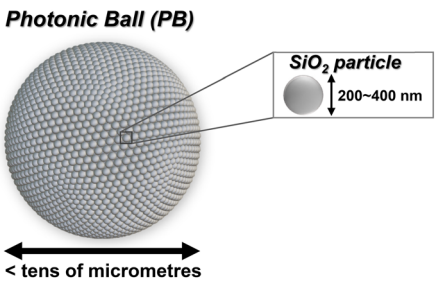

Fig. 1 Schematic diagram illustrating PB.

Several methods have been proposed for the preparation of FCC-type and onion-like PBs that involve manipulating evaporation rates.[11,25,29] Specifically, faster evaporation facilitates the formation of onion-like PBs, whereas slower evaporation favours the formation of FCC-type PBs. This variation attributed to the particle rearrangement that occurs during water evaporation from the emulsion. As water evaporates, the particles repel each other and undergo a reorganisation process; thus, a prolonged rearrangement time generally leads to a higher packing density within the PBs.[30] Despite these advances, there remains a paucity of studies on the preparation of colloidal crystalline and colloidal amorphous PBs.[28] Furthermore, PBs encounter critical issues in their application as pigments. Colloidal particles that constitute PBs interact only through weak van der Waals forces, resulting in a lack of mechanical robustness and a propensity for colour degradation owing to the collapse of the particle-assembled structure. Although various efforts have been made to enhance the mechanical robustness of structurally coloured materials in particle array systems, research specifically targeting the mechanical properties of PBs remains limited.[31–38]

In this study, we examined the effects of various experimental conditions on the particle arrangement within PBs. We focused on controlling the surface charge and electric double layer by adjusting the repulsive forces between the particles. Specifically, we investigated the influence of parameters such as the pH, ionic strength of the dispersion, and temperature during preparation. Additionally, we examined the effect of particle arrangement on their mechanical robustness, with the ultimate goal of developing PBs that exhibit enhanced mechanical robustness while maintaining their vivid structural colours.

Experimental procedures

Materials

Monodisperse SiO_2 particles used in this study were obtained from Fuji Chemical Co., Ltd. (Osaka, Japan). The particles were 200 nm in diameter and had a narrow size distribution (polydispersity index measured by dynamic light scattering: 0.033). Aqueous solutions of ammonium hydroxide (NH_4OH aq.; 28 wt%), hydrogen peroxide (H_2O_2 aq.; 30 wt%), and hydrochloric acid (HCl aq.; 1 mol dm^{-3}) and ammonium chloride (NH_4Cl) were purchased from Nacalai Tesque, Inc. (Kyoto, Japan). Tetraethyl orthosilicate (TEOS), propylene glycol, and cyclohexane were obtained from Kishida Chemical Co., Ltd. (Osaka, Japan). Hexadecane and sorbitan monooleate (Span 80) were purchased from Tokyo Chemical Industry Co. Ltd. (Tokyo, Japan). All the reagents in this study were used as received, without further purification. The water used in all experiments was purified and deionised to a resistivity of 18.2 mΩ from tap water using a Direct-Q UV water purification system (Millipore Corp., Billerica, MA, USA).

Preparation of PBs

PBs were prepared *via* the established emulsion method reported in the literature.[11] The schematic illustration of the preparation procedure of PBs was provided in Fig. S1 in the ESI.† Initially, to remove insoluble organic contaminants and to activate the Si–OH groups present on the surface of SiO_2 particles, 0.75 g of SiO_2 particles were dispersed in a mixture of H_2O, H_2O_2 aq. and NH_4OH aq. (volume ratio of 5 : 1 : 1; 20 mL) *via* ultrasonication, followed by heating at 60 °C for 1 h. Upon completion of centrifugation, the SiO_2 particles were redispersed in 40 mL of deionised water, and the supernatant was discarded. This procedure was repeated twice to ensure adequate purification. The SiO_2 dispersion was then prepared by redispersing the particles in 2.25 mL of a specifically chosen dispersant, with the pH and ionic strength of the dispersants adjusted using HCl aq., NH_4OH aq., and NH_4Cl. 100 μL of the dispersion was mixed with 900 μL of a hexadecane solution (containing 2 wt% nonionic surfactant Span 80) using a vortex mixer for 15 s, yielding a water-in-oil (W/O) emulsion. The obtained emulsion was introduced into a Teflon Petri dish containing 6 mL of the hexadecane solution (also containing 2 wt% Span 80), which had been preheated on a hot plate at 130 °C. The hot plate was maintained at this temperature for 5 h to promote the evaporation of water from the emulsion, yielding a concentrated phase. The resultant precipitate was washed four times with cyclohexane and dried to obtain PBs. To investigate the effects of the heat-treatment temperature on the particle arrangement within PBs, we used a forced convection oven as an alternative to a hot plate.

Synthesis of GMS and preparation of PBs with GMS

A water-soluble silane compound, *i.e.* glycol-modified silane (GMS; molecular structure provided in Fig. S2 in the ESI†), was synthesised using a method reported in the literature.[39] Briefly, a mixture of 0.05 mol of TEOS and 0.2 mol of propylene glycol was heated at 80 °C under reflux for 24 h. Subsequently, 0.5 μL of hydrochloric acid (10 mol dm^{-3}) was added to the reaction mixture while maintaining the refluxing conditions. The reaction was terminated by adding 50 mL of water to the solution. The synthesised GMS was then stored in a refrigerator.

For the preparation of PBs with GMS, GMS was added to the SiO_2 dispersions at a concentration of 100 mmol dm^{-3}. The subsequent procedure for preparing PBs was conducted as described above. After the PBs incorporating GMS were obtained, they were calcined in a furnace at 600 °C to convert GMS into SiO_2, interconnecting the SiO_2 particles within the PBs.

Optical characterisation of PBs

A digital camera was used to capture photographs of the PB samples. To visualise the structural colours generated by the particle-assembled structure of the PBs, we took the photographs against a black background that could absorb incoherent light scattering. The optical properties of the PBs were investigated by performing reflectance spectral measurements using an ultraviolet-visible (UV-vis) spectrophotometer (V-670; JASCO, Tokyo, Japan) equipped with an absolute reflectance measurement unit (ARMN-735).

Analysis of SiO_2 particle arrangement in PBs

The arrangement of SiO_2 particles within the PBs was examined using scanning electron microscopy (SEM; S-4800, Hitachi, Tokyo, Japan). A Voronoi diagram, *i.e.* a computational geometry analysis method,[30,40] was employed to evaluate the particle arrangement of the colloidal array materials.[41–43] Fast Fourier transform (FFT) images and Voronoi diagrams were generated from the SEM images using free software (ImageJ). An ideal colloidal crystalline particle array with a closely packed structure in the two-dimensional (2D) plane is expected to exhibit only 6-fold Voronoi polygons. Conversely, the presence of domain boundaries and/or colloidal amorphous particle array domains within PBs results in the formation of polygons with different numeric folds.

Mechanical-robustness tests of PBs

The mechanical robustness of the PBs was evaluated in terms of their resistance to ultrasonic irradiation. A schematic representation of the evaluation method is shown in Fig. 2. Upon application of ultrasonic waves to PBs dispersed in water, the assembled structure of the PBs with insufficient mechanical robustness collapsed, resulting in the isolation and dispersion of SiO_2 particles. While the PBs settle under the influence of gravity, the isolated submicron-sized SiO_2 particles remain stably suspended in the aqueous medium as colloids, leading to turbidity, which is characterised by light scattering. Consequently, the mechanical robustness of the PBs can be quantitatively assessed by monitoring their degree of light scattering.

Before the evaluation of the mechanical robustness, the PBs were heat-treated in a furnace for 1 h. Following this treatment, 0.04 g of PBs was dispersed in deionised water (3.96 mL). The dispersion was then irradiated with ultrasonic

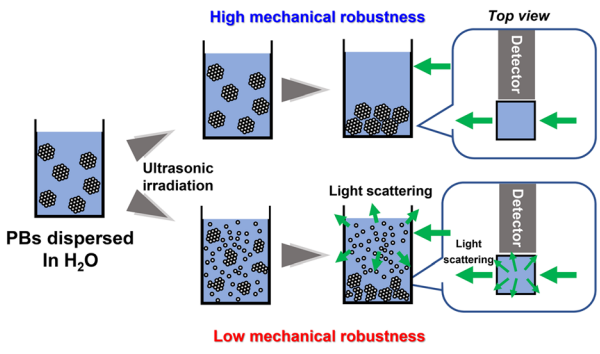

Fig. 2 Schematic representation of the mechanical-robustness test procedure for PBs involving ultrasonic irradiation.

waves using a bath-type ultrasonicator operating at 40 kHz and 160 W (Branson CPX5800-J, Emerson Electric Co., Missouri, USA). Subsequently, a portion of the dispersion (0.4 mL) was mixed with 1.6 mL of deionised water in a polystyrene cuvette and allowed to stand for 10 min. The light-scattering intensity was measured using a fluorescence spectrophotometer (FP-8600, JASCO, Tokyo, Japan) at a 90° angle relative to the incident light with a wavelength of 532 nm. The detection wavelength was set within the range 520–550 nm to determine the maximum light-scattering intensity. An increase in the disruption of PBs due to ultrasonication was correlated with a higher light-scattering intensity, indicating a reduction in the mechanical robustness of the PBs. Conversely, a lower light-scattering intensity indicated PBs with better mechanical robustness.

Results and discussion

Effects of pH of SiO_2 particle dispersions used for preparation of PBs on particle arrangement in PBs

The PBs were prepared *via* the emulsion method using dispersions of SiO_2 particles at varying pH levels to examine the effect of the pH on the particle arrangement within the PBs. In contrast to previous studies, where the pH of the SiO_2 particle dispersion used for PB preparation was often left uncontrolled,[43] in this study, we meticulously varied the pH of the dispersions using HCl aq. and NH_4OH aq. Our initial assessments spanned a broad pH range (2–11). Fig. 3 shows photographs and the corresponding UV-vis reflectance spectra of the PBs prepared from SiO_2 dispersions with pH values of 2, 3, 4, 6, 9, and 11. Each sample exhibits a striking blue structural colour when displayed against a black background. Notably, PBs derived from SiO_2 dispersions with a pH ≥ 3 exhibited a vibrant blue hue, whereas those derived from dispersions with a pH of 2 appeared to be more matte. In the reflectance spectra, all samples exhibited a peak with maximum intensity at a wavelength of *ca.* 440 nm, which is attributed to the coherent light-scattering characteristic of SiO_2 particles with a diameter of 200 nm.[16] Furthermore, the spectra of PBs prepared from SiO_2 dispersions with a pH of 3 or higher exhibited relatively sharp peaks, consistent with previous reports,[37] whereas the spectrum of PBs from the pH 2.0 dispersion exhibited a broader peak. These results

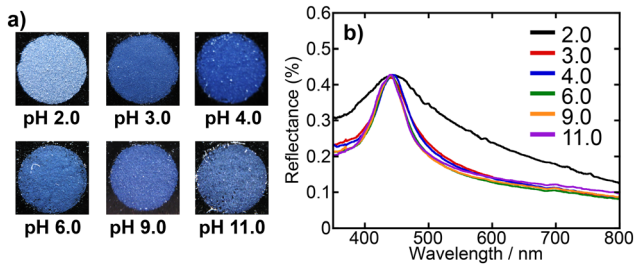

Fig. 3 a) Photographs and b) UV-vis reflectance spectra of PBs prepared from SiO_2 dispersions with pH values of 2.0, 3.0, 4.0, 6.0, 9.0, and 11.0.

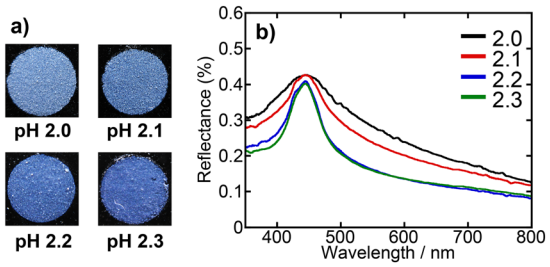

Fig. 4 a) Photographs and b) UV-vis reflectance spectra of PBs prepared from SiO_2 dispersions with pH values of 2.0, 2.1, 2.2, and 2.3.

suggest a significant variation in the particle-assembled structure of PBs depending on the preparation pH—particularly between pH values of 2 and 3. Therefore, further investigation using dispersions with pH values within this critical range is warranted.

Fig. 4 shows photographs and the corresponding UV-vis reflectance spectra of the PBs prepared from SiO_2 dispersions with pH values of 2.0, 2.1, 2.2, and 2.3. The PBs derived from dispersions with pH values of 2.2 and 2.3 exhibited colours and spectra that were nearly indistinguishable from those of PBs derived from dispersions with pH values exceeding 3.0. In contrast, the PBs produced at pH 2.1 exhibited a matte appearance and a relatively broad reflectance peak, with a further broadened peak and increased matte characteristics at pH 2.0. SEM observations of the PBs were performed to examine the particle arrangement of the samples in further detail. Fig. 5a and b present SEM images of the entire spheres and surfaces of the PBs prepared from SiO_2

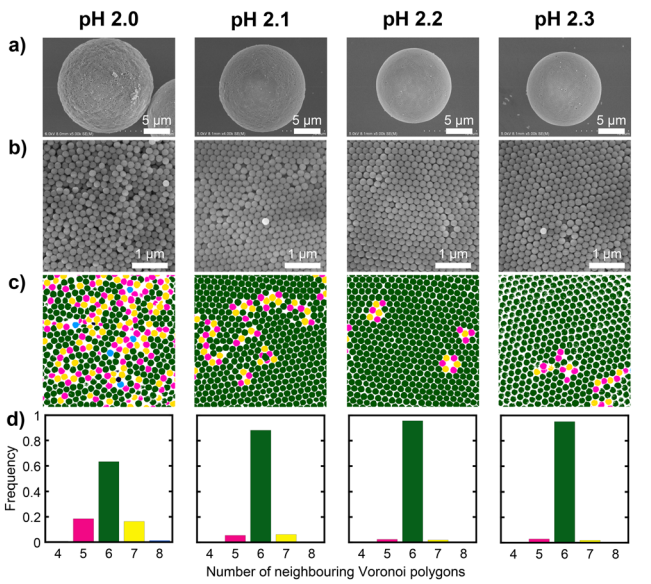

Fig. 5 SEM images of a) the entire spheres and b) surfaces of the PBs prepared from SiO_2 dispersions with pH values of 2.0, 2.1, 2.2, and 2.3. c) Voronoi diagrams obtained from SEM images and d) distributions of the number of neighbouring Voronoi polygons. Black: 4-fold polygons, pink: 5-fold polygons, green: 6-fold polygons, yellow: 7-fold polygons, blue: 8-fold polygons.

dispersions with pH values of 2.0, 2.1, 2.2, and 2.3. To eliminate the influence of the size of the PBs, observations were restricted to PBs of a unified size (*ca.* 10 μm in diameter). The obtained PBs consistently exhibited a highly spherical morphology (Fig. 5a), regardless of the pH of the dispersion used for preparation. However, a comparison of the surface smoothness revealed that the PB prepared from the pH 2.0 dispersion was relatively rough. The high-magnification images of the PBs surface shown in Fig. 5b reveal that the PBs prepared from dispersions with pH values of 2.2 and 2.3 have a nearly entirely close-packed arrangement of SiO_2 particles. At pH 2.1, while most SiO_2 particles exhibited a close-packed arrangement, some areas appeared disordered. The PBs prepared at pH 2.0 exhibited a significant change in appearance, with more than half of the particles exhibiting a disordered structure. FFT analysis of the SEM images was conducted to characterise the spatial information of the PB surfaces (Fig. S3 in the ESI†). Bright and high-order hexagonal spots, indicating well-ordered arrangements, were observed in the FFT images of the samples prepared from dispersions with higher pH values, such as 2.3. In contrast, the FFT images of the samples prepared from dispersions with lower pH values, such as 2.0 exhibited circular patterns, indicating a colloidal amorphous structure. Voronoi analysis—a well-established concept in computational geometry—was employed to quantitatively assess the regularity of the arrangement in a 2D plane. Voronoi diagrams were constructed from the SEM images (Fig. 5c) by partitioning the metric space according to the proximity of the points. Each Voronoi cell was represented as a convex polygon, with 6-fold polygons corresponding to close-packed structures, as depicted in green. The 4-fold, 5-fold, 7-fold, and 8-fold polygons are represented in black, pink, yellow, and blue, respectively. The frequencies of these polygons in each image are presented in Fig. 5d. The fractions of 6-fold polygons, indicating a colloidal crystalline arrangement, were >0.95 for PBs prepared from dispersions with higher pH values, such as 2.2 and 2.3. At pH 2.1, the PBs exhibited distinct grain boundaries (Fig. 5b), the corresponding FFT image exhibited a blurred hexagonal pattern (Fig. S3b†), and the fraction of 6-fold Voronoi polygons decreased to 0.90. For the PBs prepared from the pH 2.0 dispersion, the SiO_2 particles were presumed to form a colloidal amorphous structure, as evidenced by the Voronoi diagram, which indicated that only 60% of the polygons were 6-fold neighbours.

These results indicate that the dispersion pH affects the arrangement of SiO_2 particles within the PBs. A plausible reason for this phenomenon is the change in surface charge. Generally, the surfaces of metal oxides, including SiO_2, are covered with numerous hydroxyl (OH) groups. The surface charge of metal oxides varies with the solution pH owing to the protonation and deprotonation of the surface OH groups. The isoelectric point (IEP) of SiO_2 is approximately 2,[44] and SiO_2 particles exhibit a negative surface charge in solutions with pH values exceeding the IEP. As the solution pH approached the IEP, the surface charge diminished, reducing the repulsive force between particles and suppressing particle rearrangement during water evaporation. In the emulsion method used for the preparation of these PBs, the pH of the dispersion changed with the drying temperature. Thus, the change in particle arrangements at specific values of the zeta potential and other parameters is a complex mechanism that warrants further investigation. Nevertheless, it was demonstrated that the pH of the dispersions used for the preparation determines the surface charge of the particles, which affects the particle arrangement of the resultant PBs.

Effects of ionic strength of SiO_2 particle dispersion used for preparation of PBs on particle arrangement in PBs

To further clarify the relationship between the particle surface electric double layer and the arrangement of particles within the PBs, we prepared PBs from dispersions of SiO_2 particles with varying ionic strengths. The ionic strengths of the dispersions were meticulously adjusted to 0, 1, 10, and 100 mmol dm^{-3} through the addition of NH_4Cl. Fig. 6 presents photographs along with the corresponding UV-vis reflectance spectra of the PBs prepared from SiO_2 dispersions with various NH_4Cl concentrations. For the dispersions prepared with 0 and 1 mmol dm^{-3} NH_4Cl, the obtained PBs exhibited vivid colours and sharp reflectance peaks. As the NH_4Cl concentration increased to 10 mmol dm^{-3}, the reflectance peak broadened, and the colour transitioned to a matte finish. This trend of further broadening of the reflectance peak and increased matte surface characteristics was evident when the PBs were prepared using the dispersion containing 100 mmol dm^{-3} NH_4Cl. Fig. 7a and b present SEM images of the entire sphere and surfaces of the PBs prepared from SiO_2 dispersions with 0, 1, 10, and 100 mmol dm^{-3} NH_4Cl. The PBs consistently exhibited a spherical morphology (Fig. 7a). However, the PB prepared from the dispersion with 100 mmol dm^{-3} NH_4Cl exhibited nonspherical and misshapen characteristics. The surface SEM images of PBs prepared using dispersions with 0 and 1 mmol dm^{-3} NH_4Cl displayed colloidal crystalline-type particle

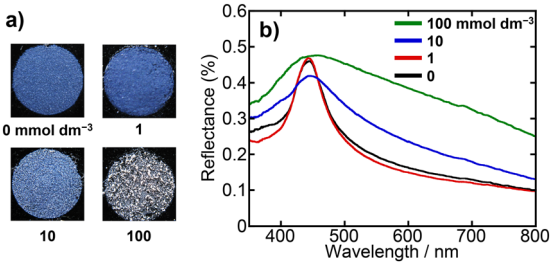

Fig. 6 a) Photographs and b) UV-vis reflectance spectra of PBs prepared from SiO_2 dispersions with NH_4Cl concentrations of 0, 1, 10, and 100 mmol dm^{-3}.

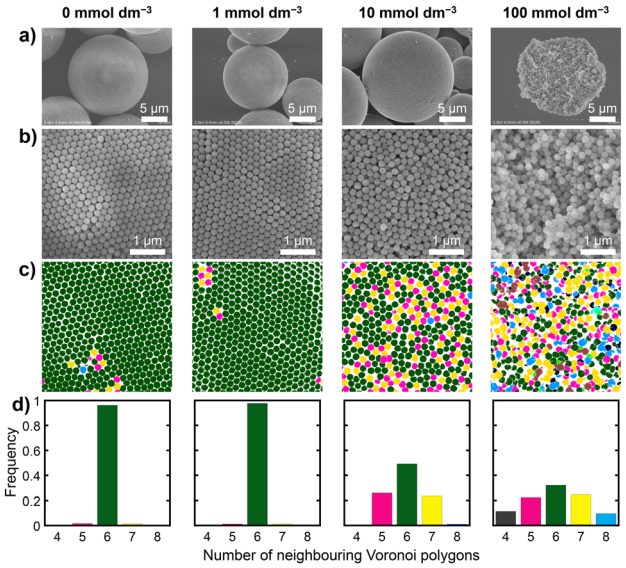

Fig. 7 SEM images of a) the entire spheres and b) surfaces of the PBs prepared from SiO_2 dispersions with NH_4Cl concentrations of 0, 1, 10, and 100 mmol dm^{-3}. c) Voronoi diagrams obtained from SEM images and d) distributions of the number of neighbouring Voronoi polygons. Black: 4-fold polygons, pink: 5-fold polygons, green: 6-fold polygons, yellow: 7-fold polygons, blue: 8-fold polygons.

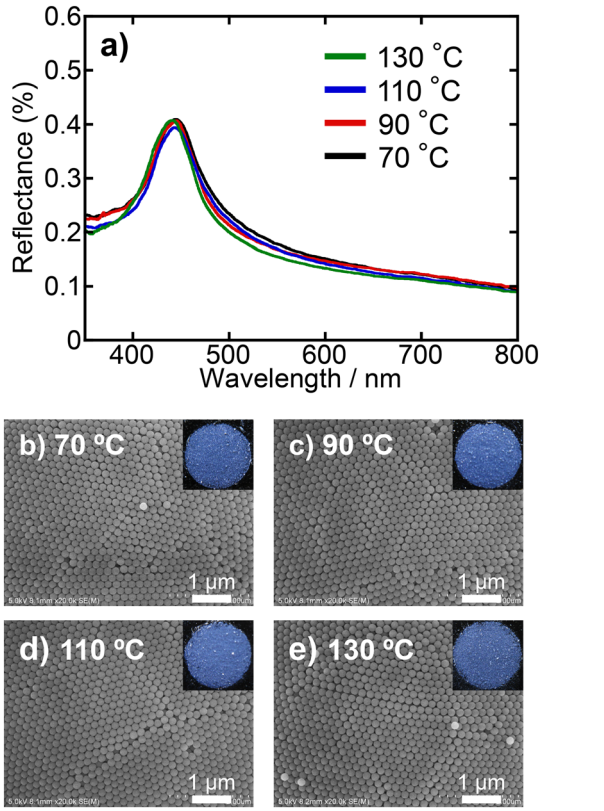

Fig. 8 a) UV-vis reflectance spectra and b–e) surface SEM images of PBs prepared at drying temperatures of 70, 90, 110, and 130 °C using SiO_2 dispersions devoid of the ionic additive. Photographs of PBs are provided as insets in the SEM images.

arrangements (Fig. 7b). Bright, highly ordered hexagonal spots, indicating well-ordered arrangements, are observed in the corresponding FFT images (Fig. S4 in the ESI†). Furthermore, the corresponding Voronoi diagrams exhibited a fraction of 6-fold polygons exceeding 0.95, with a minimal presence of 5- and 7-fold polygons (Fig. 7c and d). In the case of 10 mmol dm^{-3} NH_4Cl, the SEM image indicated colloidal amorphous-type particle arrangements (Fig. 7b). The corresponding FFT image displays a ring pattern (Fig. S4b†), suggesting the presence of only short-range order in the arrangement of the particles. The Voronoi diagrams revealed a fraction of 6-fold polygons of approximately 0.5, with considerably more 5- and 7-fold polygons. Additionally, in the case of 100 mmol dm^{-3} NH_4Cl, the hexagonal spots in the FFT image were completely obscured, and the fraction of 6-fold polygons was reduced in the Voronoi diagram. These observations are attributed to alterations in the repulsive force between particles as the thickness of the electric double layer changed with the ionic strength. This underscores the notion that the ionic strength of the dispersion provides precise control of the particle arrangement within PBs.

Effects of drying temperature on particle arrangement in PBs

The effects of drying temperature during the preparation of PBs on particle arrangement in PB were investigated by varying the rate of water evaporation from the droplets in the W/O emulsion. Both dispersions without and with the ionic additive (10 mmol dm^{-3} NH_4Cl) were examined. Drying conditions were 70, 90, 110, and 130 °C for 10, 5, 5, and 2 h, respectively. Fig. 8 shows the reflectance spectra and surface SEM images of PBs prepared at various drying temperatures using a dispersion without ionic additives. The photographs of the PBs, which are included as insets in the SEM images, confirmed the colour appearance of the PBs. Remarkably, there were almost no discernible differences in the reflectance spectra across the different drying conditions (Fig. 8a). Colloidal crystalline-type particle arrangements and vivid colours were consistently observed in the surface SEM images and photographs, respectively, under all drying conditions (Fig. 8b–e). Furthermore, the Voronoi diagrams and FFT images corroborate the formation of colloidal crystalline-type particle arrangements (Fig. S5 in the ESI†). The PBs prepared using dispersions containing ionic additives exhibited a significantly different trend. Fig. 9 shows the reflectance spectra and surface SEM images of PBs prepared at various drying temperatures using SiO_2 dispersions with NH_4Cl (10 mmol dm^{-3}). At a drying temperature of 70 °C, the resultant PBs exhibited vibrant colours and a sharp peak in the reflectance spectrum (Fig. 9a and b), similar to the results obtained for PBs prepared without ionic additives. However, as the drying temperature increased, the colour transitioned to a matte finish, and the reflectance peak broadened, indicating that the PBs possessed a colloidal amorphous-type particle

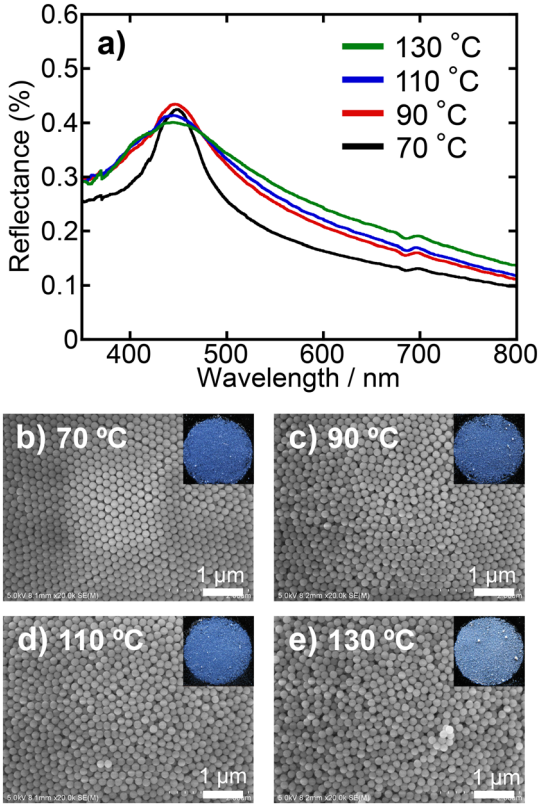

Fig. 9 a) UV-vis reflectance spectra and b–e) surface SEM images of PBs prepared at drying temperatures of 70, 90, 110, and 130 °C using SiO_2 dispersions with NH_4Cl (10 mmol dm^{-3}). Photographs of PBs are provided as insets in the SEM images.

arrangement, as discussed above. The Voronoi diagrams and FFT images further indicated the formation of colloidal amorphous-type particle arrangements (Fig. S6 in the ESI†). These findings suggested that the drying temperature significantly affected the evaporation rate of water from the droplets within the emulsions. Elevated drying temperatures accelerate evaporation, reducing the amount of time available for particle rearrangement. The results indicated that for dispersions without ionic additives, the drying temperature had a relatively minor effect on the particle arrangement, primarily owing to the strong electrostatic repulsion between the SiO_2 particles. Conversely, when dispersions containing ionic additives at a certain concentration are employed, it has been clarified that differences in drying temperature result in changes in the arrangement of SiO_2 particles in the resultant PBs, indicating that the duration of water evaporation from the emulsion affects the arrangement of SiO_2 particles within the PBs. In conclusion, since the process of water evaporation and subsequent particle rearrangement essentially depends on the drying temperature, the drying temperature is also a pivotal factor in determining the particle arrangement of PB, especially when the electrostatic repulsion between particles is suppressed to a certain extent by the increase in ionic strength.

Effects of particle arrangement on mechanical robustness of PBs

The mechanical robustness of the PBs was evaluated by measuring the extent to which the SiO_2 particles detached from the PBs when dispersed in water and subjected to ultrasonic irradiation. PBs with colloidal amorphous-type arrangements (prepared using a dispersion of SiO_2 particles with a pH of 2) and colloidal crystalline-type arrangements (prepared using a dispersion of SiO_2 particles with a pH of 3) were employed to examine the mechanical robustness. Prior to the examinations, the PB samples were heat-treated at 800 °C. Following heat treatment, a portion of each sample was dispersed in water and subsequently irradiated with ultrasound. Fig. 10a presents the light-scattering intensity of the PB dispersion as a function of the ultrasonication duration. As described in the Experimental procedures section, light scattering arises from isolated SiO_2 particles and oligomeric aggregates that fragment from the PBs; thus, an increase in scattering intensity indicates the collapse of the PBs. The light scattering intensities before ultrasonic irradiation were 8.4 and 11.0 for the dispersions of colloidal amorphous-type PBs and crystalline type PBs, respectively (plots not given). For the colloidal amorphous-type PBs, the light-scattering intensity gradually increased with an increase in the sonication time, indicating poor mechanical robustness against ultrasonic irradiation. Fig. 10b displays SEM images of PBs with colloidal amorphous-type arrangement and colloidal crystalline-type arrangement after ultrasonic irradiation for 180 min. These SEM images revealed that while the PBs retained some of their spherical shapes, numerous SiO_2 particles detached from the surface,

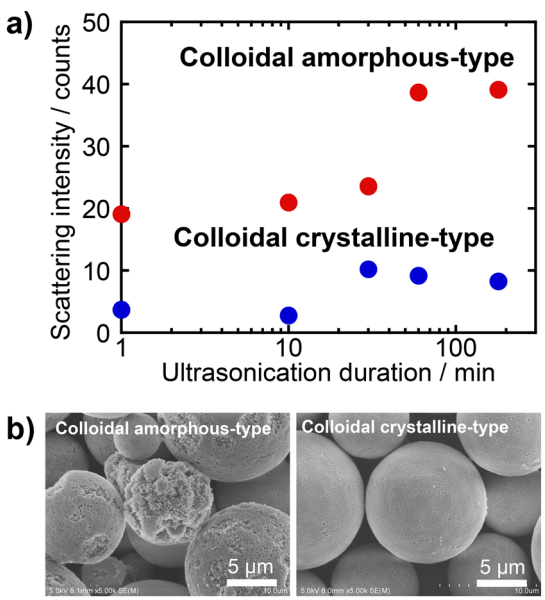

Fig. 10 a) Changes in the light-scattering intensity of the PB dispersion as a function of the ultrasonication duration and b) SEM images of PBs with colloidal amorphous-type and colloidal crystalline-type arrangements after ultrasonic irradiation for 180 min.

clearly suggesting the collapse of the PBs. In contrast, the intensity of light scattering due to the dispersion of colloidal crystalline-type PBs remained low even after 180 min. Notably, the shape of the colloidal crystalline-type PBs did not change during the ultrasonic irradiation.

The observed differences in the mechanical robustness in response to ultrasonic irradiation are attributed to the packing density of the SiO_2 particles within the PBs. The colloidal crystalline particle arrangement had a higher packing density than its colloidal amorphous counterparts. Consequently, the colloidal amorphous-type PBs maintained a larger free volume, resulting in increased vibrational motion and subsequent collapse. Additionally, necking formations occurred between SiO_2 particles during the heat treatment at 800 °C. Densely packed colloidal crystalline PBs exhibited more interparticle necking than their loosely packed colloidal amorphous counterparts (Fig. S7 in the ESI†), which significantly enhanced their mechanical robustness. Consequently, the robustness of the colloidal crystalline-type PBs was markedly superior to that of the colloidal amorphous-type PBs. In our previous study,[37] coatings with colloidal crystalline-type arrays exhibited superior resilience to those with colloidal amorphous-type arrays in both ultrasonic irradiation and sandpaper abrasion tests. The present findings support this trend, confirming that particle arrangement is a fundamental factor affecting the robustness of particle array-type structurally coloured materials.

Preparation of PBs with enhanced mechanical robustness

In colloidal assemblies, colloidal crystalline arrangements exhibit superior mechanical robustness to their amorphous counterparts—particularly for heat-treated PBs. Our objective was to achieve an even greater degree of mechanical robustness in colloidal crystalline PBs. In our previous studies,[14,37,38] we established that the inclusion of binders to bond SiO_2 particles within the arrays significantly enhances their mechanical robustness. Consequently, we aimed to improve the necking phenomenon that occurs during heat treatment by incorporating an appropriate binder.

The binder must possess water solubility, as it needs to be introduced into the aqueous phase of the emulsion, specifically the SiO_2 particle dispersion, to be effectively integrated within the PBs. Furthermore, ionic and acidic characteristics should be avoided to preserve the integrity of colloidal crystalline PBs. Considering these criteria, we focused on the water-soluble silane compound, GMS, developed by Kakihana *et al.*[39] GMS can be converted into SiO_2 upon heat treatment, and its incorporation into PBs facilitates the enhanced formation of necks between particles. For the preparation of PBs, GMS was added to the SiO_2 dispersion at a concentration of 100 mmol dm^{-3}. Reflectance spectra and SEM images of the resulting samples are shown in Fig. S8 in the ESI.† The PBs exhibited vivid blue structural colours regardless of the addition of GMS, and the

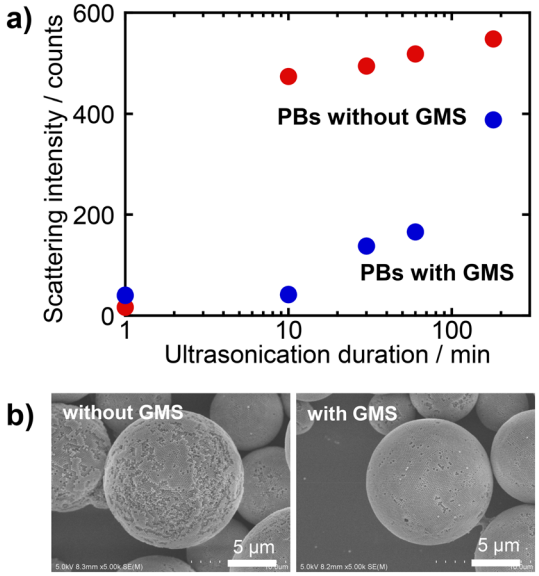

Fig. 11 a) Changes in the light-scattering intensity of the PB dispersion as a function of the ultrasonication duration and b) SEM images of PBs prepared with and without GMS after ultrasonic irradiation for 180 min.

particle arrangement remained consistent with that of the colloidal crystalline type. Thus, it was confirmed that the addition of nonionic GMS has a negligible effect on the rearrangement of SiO_2 particles during the formation of the PBs, as expected. The mechanical robustness was evaluated through ultrasonication tests performed on samples subjected to heat treatment at 600 °C. As previously discussed, the mechanical robustness of colloidal crystalline-type PBs can be significantly enhanced by heat treatment at 800 °C. However, depending on the specific applications and the particles employed for PB preparation, high-temperature heat treatment may be unsuitable in certain cases.[45] Therefore, we selected a heat-treatment temperature of 600 °C, at which GMS is completely converted into SiO_2. The results of the mechanical-robustness tests for the PBs with and without GMS are presented in Fig. 11. The PBs prepared with GMS exhibited significantly lower light-scattering intensity after ultrasonic irradiation than the PBs prepared without GMS, indicating less SiO_2 particle detachment from the PBs (Fig. 11a). Additionally, in the SEM images, the PBs with GMS exhibited less collapse than those without GMS (Fig. 11b). These findings suggest that the inclusion of GMS contributes to the formation of stronger necking between SiO_2 particles within the PBs by heat treatment. Consequently, it is feasible to prepare colloidal crystalline PBs with vivid colours and enhanced robustness, even at low heat-treatment temperatures.

Conclusions

We investigated the effects of preparation parameters, such as the pH and ionic strength of the SiO_2 particle dispersion,

on the particle arrangement and mechanical robustness of PBs. The particle arrangement of PBs exhibited significant changes depending on the pH. When PBs were prepared under conditions close to the IEP of the substance used for the particles (approximately 2 in the case of SiO_2), colloidal amorphous-type structures were predominantly obtained. Conversely, at pH values far from the IEP, colloidal crystal structures were observed. Regarding the ionic strength of the SiO_2 particle dispersion, the addition of 1 mmol dm^{-3} of NH_4Cl had negligible effect; however, the addition of $\geq$10 mmol dm^{-3} of NH_4Cl increased the likelihood of the PBs having a colloidal amorphous structure. At this ionic strength, the temperature at which water evaporated from the emulsion had a pronounced effect; a low drying temperature favoured a colloidal crystalline structure, whereas a high drying temperature resulted in a colloidal amorphous structure. The differences in the resulting arrangement state are attributed to the surface charge of the SiO_2 particles and the state of the electric double layer, which affects the ease of particle rearrangement owing to the capillary forces associated with water evaporation. The colloidal crystalline PBs exhibited a vivid colour, whereas the colloidal amorphous PBs exhibited a matte colour, indicating that both the particle arrangement and colour in the PBs can be precisely controlled by varying the dispersion medium and the conditions of water evaporation during preparation. Furthermore, regarding heat-treated PBs, colloidal crystalline-type PBs exhibited superior mechanical robustness compared to their colloidal amorphous-type counterparts. This enhancement is attributed to neckings between neighbouring particles, which results from the differences in the packing density of the PBs. Moreover, PBs prepared with GMS as a binder exhibited far higher mechanical robustness, even when subjected to heat treatment at lower temperatures. Therefore, the PBs developed in this study, which are characterised by controlled colouration and improved mechanical robustness, hold considerable promise as alternatives to conventional inorganic pigments.

Data availability

Raw data were generated at Hiroshima University. The data that support the findings of this study are available from the corresponding author, K. K., upon reasonable request.

Author contributions

TY: investigation, writing – original draft; YN: investigation; KI: investigation; NT: methodology, writing – review & editing; KK: conceptualization, funding acquisition, methodology, supervision, writing – review & editing; KI: supervision; YT: methodology, resources.

Conflicts of interest

There are no conflicts to declare.

Acknowledgements

This work was supported by JSPS KAKENHI Grant Numbers JP18K19132, JP20H02439, JP22H05143, JP23H00236, JP23KJ1644, and JP24K21793. This work was also supported by the Murata Science and Education Foundation, Grant Number M24AN128. T. Y. was supported by JST, the establishment of university fellowships towards the creation of science technology innovation, Grant Number JPMJFS2129.

References

1 K. Nassau, *The Physics and Chemistry of Color: The Fifteen Causes of Color*, John Wiley & Sons, Inc., New York, NY, USA, 2nd edn, 2001.
2 R. G. Kuehni, *Color: An Introduction to Practice and Principles*, John Wiley & Sons, Inc., Hoboken, NJ, USA, 2nd edn, 2005.
3 A. L. Wani, A. Ara and J. A. Usmani, *Interdiscip. Toxicol.*, 2015, **8**, 55–64.
4 S. H. Gilani and M. Marano, *Environ. Res.*, 1979, **19**, 427–431.
5 N. Rustagi and R. Singh, *Indian J. Occup. Health*, 2010, **14**, 45.
6 S. Kinoshita, S. Yoshioka and J. Miyazaki, *Rep. Prog. Phys.*, 2008, **71**, 076401.
7 Y. Zhao, Z. Xie, H. Gu, C. Zhu and Z. Gu, *Chem. Soc. Rev.*, 2012, **41**, 3297.
8 M. Kambe, D. Xhu and S. Kinoshita, *J. Phys. Soc. Jpn.*, 2011, **80**, 054801.
9 F. Marlow, Muldarisnur, P. Sharifi, R. Brinkmann and C. Mendive, *Angew. Chem., Int. Ed.*, 2009, **48**, 6212–6233.
10 H. Fudouzi and Y. Xia, *Langmuir*, 2003, **19**, 9653–9660.
11 M. Sakai, T. Seki and Y. Takeoka, *Small*, 2018, **14**, 1800817.
12 Y. Takeoka, *J. Mater. Chem.*, 2012, **22**, 23299.
13 K. Katagiri, Y. Tanaka, K. Uemura, K. Inumaru, T. Seki and Y. Takeoka, *NPG Asia Mater.*, 2017, **9**, e355.
14 K. Katagiri, K. Uemura, R. Uesugi, K. Inumaru, T. Seki and Y. Takeoka, *RSC Adv.*, 2018, **8**, 10776–10784.
15 M. Harun-Ur-Rashid, A. Bin Imran, T. Seki, M. Ishii, H. Nakamura and Y. Takeoka, *ChemPhysChem*, 2010, **11**, 579–583.
16 Y. Takeoka, S. Yoshioka, A. Takano, S. Arai, K. Nueangnoraj, H. Nishihara, M. Teshima, Y. Ohtsuka and T. Seki, *Angew. Chem., Int. Ed.*, 2013, **52**, 7261–7265.
17 M. Sakai, H. Kim, Y. Arai, T. Teratani, Y. Kawai, Y. Kuwahara, K. Abe, Y. Kuwana, K. Ikeda, K. Yamada and Y. Takeoka, *ACS Appl. Nano Mater.*, 2020, **3**, 7047–7056.
18 R. Ohnuki, M. Sakai, Y. Takeoka and S. Yoshioka, *Langmuir*, 2020, **36**, 5579–5587.
19 S.-H. Kim, S.-J. Jeon and S.-M. Yang, *J. Am. Chem. Soc.*, 2008, **130**, 6040–6046.
20 S.-H. Kim, S. Y. Lee, G.-R. Yi, D. J. Pine and S.-M. Yang, *J. Am. Chem. Soc.*, 2006, **128**, 10897–10904.
21 V. Rastogi, S. Melle, O. G. Calderón, A. A. García, M. Marquez and O. D. Velev, *Adv. Mater.*, 2008, **20**, 4263–4268.
22 R. Ohnuki, S. Isoda, M. Sakai, Y. Takeoka and S. Yoshioka, *Adv. Opt. Mater.*, 2019, **7**, 1900227.

23 J. H. Moon, G.-R. Yi, S.-M. Yang, D. J. Pine and S. B. Park, *Adv. Mater.*, 2004, **16**, 605–609.
24 Z. Yu, L. Chen and S. Chen, *J. Mater. Chem.*, 2010, **20**, 6182.
25 N. Vogel, S. Utech, G. T. England, T. Shirman, K. R. Phillips, N. Koay, I. B. Burgess, M. Kolle, D. A. Weitz and J. Aizenberg, *Proc. Natl. Acad. Sci. U. S. A*, 2015, **112**, 10845–10850.
26 O. D. Velev, A. M. Lenhoff and E. W. Kaler, *Science*, 2000, **287**, 2240–2243.
27 R. Ohnuki, N. Kunimoto, Y. Takeoka and S. Yoshioka, *Part. Part. Syst. Charact.*, 2022, **39**, 2100257.
28 R. Ohnuki, Y. Takeoka and S. Yoshioka, *ACS Appl. Nano Mater.*, 2023, **6**, 13137–13147.
29 J. Wang, C. F. Mbah, T. Przybilla, B. Apeleo Zubiri, E. Spiecker, M. Engel and N. Vogel, *Nat. Commun.*, 2018, **9**, 5259.
30 T. Nishida, K. Sugihara and M. Kimura, *J. Comput. Appl. Math.*, 2007, **202**, 377–391.
31 Q. Li, Y. Zhang, L. Shi, H. Qiu, S. Zhang, N. Qi, J. Hu, W. Yuan, X. Zhang and K.-Q. Zhang, *ACS Nano*, 2018, **12**, 3095–3102.
32 Y. Meng, B. Tang, B. Ju, S. Wu and S. Zhang, *ACS Appl. Mater. Interfaces*, 2017, **9**, 3024–3029.
33 B. Xu, Q. Xu, M. Hou, J. Su, H. Zhang, X. Lu and Z. Ni, *Dyes Pigm.*, 2023, **218**, 111522.
34 D. Yoshioka, K. Kishikawa and M. Kohri, *Nanomaterials*, 2022, **12**, 3338.
35 X. Shi, J. He, X. Xie, R. Dou and X. Lu, *Dyes Pigm.*, 2019, **165**, 137–143.
36 M. Pan, X. bai Li, C. Xiong, X. Chen, L. Wang, X. Chen, L. Pan, H. Xu, J. Zhao and Y. Li, *Part. Part. Syst. Charact.*, 2020, **37**, 1900495.
37 T. Yamanaka, N. Tarutani, K. Katagiri, K. Inumaru and Y. Takeoka, *Adv. Eng. Mater.*, 2024, **26**, 2400814.
38 K. Katagiri, K. Uemura, R. Uesugi, N. Tarutani, K. Inumaru, T. Uchikoshi, T. Seki and Y. Takeoka, *ACS Appl. Mater. Interfaces*, 2020, **12**, 40768–40777.
39 M. Kakihana, *J. Ceram. Soc. Jpn.*, 2009, **117**, 857–862.
40 F. Aurenhammer, *ACM Comput. Surv.*, 1991, **23**, 345–405.
41 A. Huerta, G. G. Naumis, D. T. Wasan, D. Henderson and A. Trokhymchuk, *J. Chem. Phys.*, 2004, **120**, 1506–1510.
42 A. Kawamura, M. Kohri, S. Yoshioka, T. Taniguchi and K. Kishikawa, *Langmuir*, 2017, **33**, 3824–3830.
43 N. Tarutani, K. Kawaguchi, K. Katagiri and K. Inumaru, *J. Sol-Gel Sci. Technol.*, 2022, **104**, 456–463.
44 K. Hasegawa, M. Tatsumisago and T. Minami, *J. Ceram. Soc. Jpn.*, 1997, **105**, 569–572.
45 T. Yamanaka, N. Tarutani, K. Katagiri, K. Inumaru, Y. Takeoka and T. Masui, *ACS Appl. Mater. Interfaces*, 2022, **14**, 29324–29330.